Letter

Intracellular Messenger RNA Triggered Catalytic Hairpin Assembly for Fluorescence Imaging Guided Photothermal Therapy

fengxia su, Cheng-Xiong Yang, and Xiu-Ping Yan

Anal. Chem., **Just Accepted Manuscript** • DOI: 10.1021/acs.analchem.7b01348 • Publication Date (Web): 29 Jun 2017

Intracellular Messenger RNA Triggered Catalytic Hairpin Assembly for Fluorescence Imaging Guided Photothermal Therapy

Feng-Xia Su,[†] Cheng-Xiong Yang[†] and Xiu-Ping Yan[*,†,‡]

[†]College of Chemistry, Research Center for Analytical Sciences, State Key Laboratory of Medicinal Chemical Biology, and Tianjin Key Laboratory of Molecular Recognition and Biosensing, Nankai University, 94 Weijin Road, Tianjin 300071, China *Fax: +86-22-23506075. E-mail: xpyan@nankai.edu.cn

[‡]Collaborative Innovation Center of Chemical Science and Engineering (Tianjin), 94 Weijin Road, Tianjin 300071, China

ABSTRACT: We show a theranostic nanoplatform for messenger RNA (mRNA) triggered enhanced fluorescence imaging guided therapy. Catalytic hairpin assembly (CHA) and gold nanorods (AuNRs) are employed to fabricate the theranostic nanoplatform. Two hairpin DNAs and Cy5 labeled duplex DNA are integrated into the CHA for mRNA triggered fluorescence signal amplification via hybridization and displacement with mRNA. The AuNRs act both as the fluorescence quencher and the photothermal therapy (PTT) agent. The nanoplatform not only enables sensitive and specific imaging of target mRNA in living cells and good differentiating of the survivin mRNA expression levels in different cell lines, but also offers excellent photothermal conversion efficiency for PTT. The developed nanoplatform has great potential for sensitive and specific intracellular mRNA imaging guided PTT.

Messenger RNA (mRNA), as a transcription product of genomic DNA and translation template of protein, has been employed as a biomarker for early diagnosis and precision treatment due to its critical role in life process.[1-3] Furthermore, differentiation of mRNA expression levels will provide valuable information for medical diagnosis and therapy method.[4,5] Antisense oligonucleotide is commonly used for intracellular mRNA imaging based on the binding with specific region of target mRNA.[6-8] Integrating therapeutic function and intracellular mRNA imaging into a single platform has potential for personalized medicine. So, intracellular mRNA imaging based theranostic platforms have been developed, such as upconversion nanobeacons for mRNA imaging guided drug therapy,[9] Fe_3O_4@polydopamine core-shell nanocomposites for mRNA Imaging guided photothermal therapy (PTT),[10] and molecular beacons for mRNA activated photodynamic therapy (PDT).[11,12] However, such intracellular mRNA imaging based theranostic platforms suffer insufficient fluorescence sensitivity due to the one-to-one binding.

In vitro amplification of mRNA based on enzyme reactions, such as reverse transcription-polymerase chain reaction (RT-PCR),[13,14] rolling circle amplification (RCA),[15,16] and loop-mediated isothermal amplification (LAMP),[17] enables enormous signal enhancement, but is improper for intracellular mRNA detection. Enzyme-free amplification, such as catalytic hairpin assembly (CHA) and hybridization chain reaction (HCR) based methods, therefore, has been developed for mRNA imaging in cancer cells or sectioned zebrafish embryos.[18-23] CHA as an enzyme free signal enhancement circuit, depends on the hybridization and displacement of two hairpin DNAs in isothermal condition.[24,25] This promising circuit has been further adapted for a variety of applications, such as analysis of nucleic acid and small molecule.[26] Nevertheless, integrating enzyme-free amplification into a theranostic nanoplatform for sensitive mRNA imaging guided therapy has not been reported yet.

Herein, we show the design and fabrication of a CHA based theranostic nanoplatform for sensitive and specific intracellular mRNA triggered fluorescence guided therapy. In the theranostic nanoplatform, we employ Cy5 labeled duplex DNA as the near-infrared (NIR) fluorescence reporter of CHA, and AuNRs as the fluorescence quencher and PTT agent due to the strong surface plasmon absorption at NIR region and high photothermal conversion efficiency.[27-29] We also assemble two intracellular mRNA triggerable hairpin DNAs to the Cy5 labeled duplex DNA on the surface of AuNRs to enable fluorescence amplification. The fluorescence of Cy5 keeps "off" state in the absence of target mRNA, and turns "on" by target mRNA triggering. The "off" to "on" process effectively avoids the "false positive" signal in the always-on systems. Thus, the "off" to "on" theranostic nanoplatform offers synergistic advantages of enzyme free signal amplification from CHA and the high photothermal effect from AuNRs for mRNA triggered fluorescence imaging guided PTT.

Figure 1 shows the design and fabrication of the AuNRs-based CHA (ACHA) theranostic nanoplatform. AuNRs were

synthesized by a seed-mediated growth method.[30] As shown in Figure 1A, 5′-GTCCGATATAGCAACCTTTT-3′-SH (R_b-SH, e*-f*) is functionalized on the surface of AuNRs through Au-S bond.[31] Hybridizing region f-e of Cy5-5′-GGTTGCTATATCGGACAGAGATG-3′ (R_a-Cy5, f-e-b) with region e*-f* of R_b-SH on the surface of AuNRs gave a fluorescence-silence complex AuNR-R_{ab}-Cy5 owing to the overlap between the absorption spectra of AuNRs and the fluorescence spectra of Cy5. Two hairpin DNA strands 5′-TTGAATGTAGAGATGCGGTGGTCCCGTCTTGAGCGAC CACCGCATCTCTGTCCGATATAGCAACC-3′ (H_1, a-b-c-d-c*-b*-e*-f*) and 5′-CGGTGGTCGCTCAAGACGGGACCACCGCATCTCTCC GTCTTGAGC-3′ (H_2, c-d*-c*-b*-d) are rationally designed to assemble with R_{ab}-Cy5 on AuNRs to amplify the fluorescence signal. Finally, H_1, H_2 and AuNR-R_{ab}-Cy5 were packed into transfect reagent H4000 to obtain the transfection complex for their easy delivery into cells.

Figure 1B illustrates the principle of the CHA based theranostic nanoplatform. Survivin mRNA, overexpressed in many malignancies,[32] was chosen as the model target. Once transfection complex is endocytosed into cells, survivin mRNA (c*-b*-a*) expressed in cytoplasm hybridizes with exposed region a of H_1, and then displaces region c*-b*, leading to H_1 unfolding and H_1-mRNA forming. The released region d-c* of H_1 hybridizes with exposed region c of H_2, further with region d*, generating the metastable tripolymer of H_1-mRNA-H_2. mRNA is displaced by region c*-b* of H_2, and employed for next cycle. In the same way, the region b*-e*-f* of H_1-H_2 full complementary to R_a-Cy5 (f-e-b) can displace R_b-SH to yield stable H_1-H_2-R_a-Cy5 and turn fluorescence "on". The mRNA can trigger multiple cycles to generate H_1-H_2, and H_1-H_2-R_a-Cy5 to enhance the fluorescence.Then, 808 nm NIR light irradiates on intracellular AuNR-R_{ab}-Cy5 in cells for PTT.

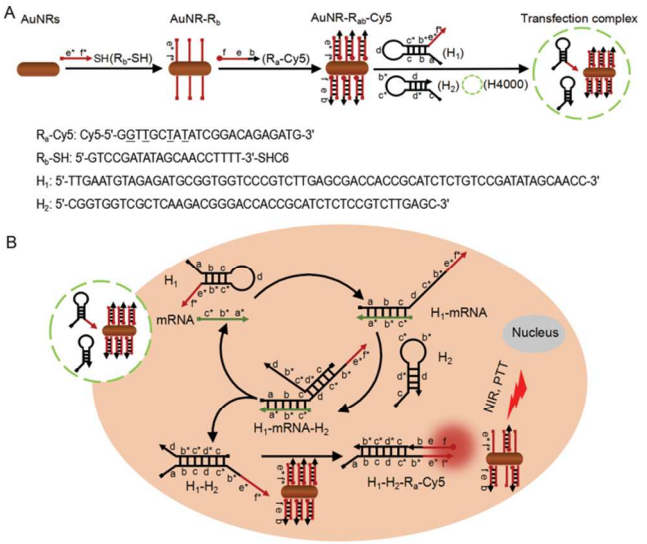

Figure 1. (A) Synthesis of transfection complex, and sequences of DNA strands. Note: The underlined bases are locked nucleic acids (LNA). (B) Schematic representation of CHA-based theranostic nanoplatform for mRNA triggered fluorescence imaging guided PTT. At the end of DNA strand, the quadrate represents the 5′ end, and arrow represents the 3′ end. Different regions of the DNA strands and their corresponding complementary regions are termed with letters a-f and a*-f*, respectively (see Table S1 for details).

Transmission electron microscopic (TEM) image reveals the prepared AuNRs have an average length of 46.77 nm and diameter of 15.83 nm with an aspect ratio of 2.95 (Figure 2A). The AuNRs exhibit a Zeta potential of +44.5 mV due to the positive charged cetyl-trimethyl ammonium bromide (CTAB) on the surface. The R_{ab}-Cy5 functionalization of the AuNRs leads to a Zeta potential of -9.7 mV due to the negative charge of DNA phosphate backbone (Figure 2B).

The prepared AuNRs possess two main absorption peaks at 716 nm and 521 nm, while AuNR-R_{ab}-Cy5 shows an additional absorption peak of DNA at 260 nm (Figure 2C). As the maximum absorption peak of the AuNRs does not overlap the maximum fluorescence emission peak of Cy5, AuNRs is not the best quencher to Cy5. However, due to the longitudinal absorption peak of AuNRs from 605 nm to 840 nm overlaps the maximum fluorescence emission peak of Cy5 at 665 nm (Figure S1), AuNRs is still an effective quencher to the fluorescence of Cy5 as the fluorescence intensity of AuNR-R_{ab}-Cy5 decreases obviously compared with that of R_a-Cy5 (Figure S2). The therapeutic efficacy of PTT is closely related to the thermal output of AuNRs. 808 nm laser irradiation led to an obvious temperature rise (approximately 40 ^{o}C) in 10 min both in AuNRs and AuNR-R_{ab}-Cy5 solution (Figure 2D). Meanwhile, the increasing temperature of AuNR-R_{ab}-Cy5 solution caused the fluorescence "on" of the fluorescence-silenced AuNR-R_{ab}-Cy5 due to the denaturation of the duplex R_{ab}-Cy5 (Figure S2).

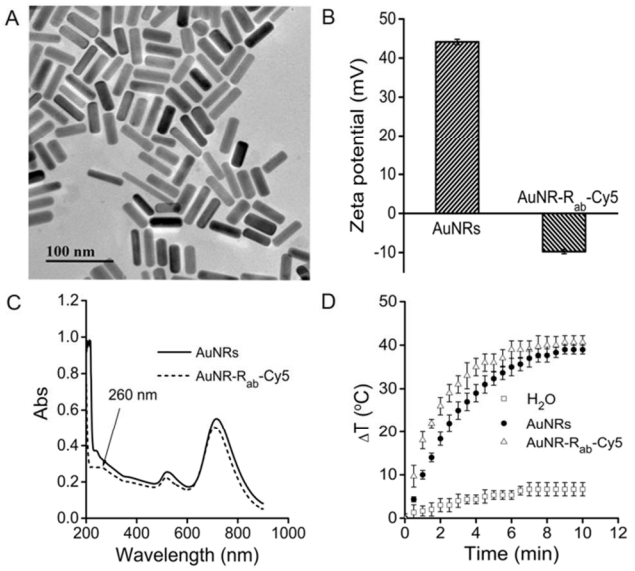

Figure 2. (A) TEM image of AuNRs. (B) Zeta potential of AuNRs and AuNR-R_{ab}-Cy5. (C) Absorption spectra of AuNRs and AuNR-R_{ab}-Cy5. (D) Temperature change of H_2O, AuNRs and AuNR-R_{ab}-Cy5 solution during NIR laser irradiation.

To show the rationality of the ACHA theranostic nanoplatform, the two hairpin DNAs (H_1 and H_2) with or without 5′-GACCACCGCATCTCTACATTCAA-3′ DNA target analogue of survivin mRNA were separated on polyacrylamide gel electrophoresis (PAGE) gel (Figure 3A). No interaction between H_1 and H_2 was observed in the absence of DNA target (Lane 4). The presence of DNA target initiates the reaction to generate duplex of H_1-H_2 (Lane 6), which is in accordance with the annealing of H_1-H_2 (Lane 5). The result demonstrates the rationality of hairpin structure design and feasibility of the ACHA theranostic nanoplatform.

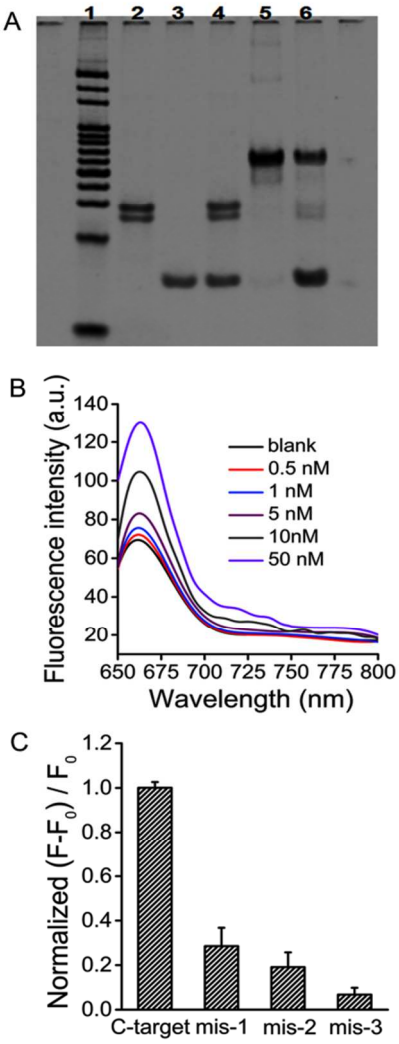

Figure 3. (A) PAGE separation image of the hairpin DNAs (H_1 and H_2) and CHA reaction product. Lane 1: 20 bp DNA ladder marker; Lane 2: H_1; Lane 3: H_2; Lane 4: H_1 and H_2; Lane 5: annealing of H_1-H_2; Lane 6: CHA reaction product. (B) Fluorescence enhancement of ACHA strategy with variety of target concentrations under excitation at 610 nm. (C) Normalizded fluorescence enhancement of ACHA with C-target, mis-1, mis-2, and mis-3 target. Note: F and F_0 represent the fluorescence intensity of ACHA product with 10 nM corresponding target, and that of ACHA product without target, respectively.

A series of DNA target solutions from 0.5 nM to 50 nM were used to test the sensitivity of the ACHA theranostic nanoplatform. The fluorescence intensity at 670 nm increased with the DNA target concentration (Figure 3B). Meanwhile, complementary DNA target (C-target), two mismatched (mis-2) and three mismatched (mis-3) DNA target were employed to verify the specificity of the ACHA theranostic nanoplatform. The result demonstrates the excellent differentiation ability between C-target and mis-1 (3.5-fold), mis-2 (5.3-fold), or mis-3 (14.9-fold) DNA target (Figure 3C).

The ACHA nanoplatform was then applied for survivin mRNA imaging in living cell. As the degradation of synthesized DNAs by lysosome may lead to a high signal background for cell study, we mingled four LNAs modified nucleotides in R_a-Cy5 to resist nuclease digestion. The stability of AuNR-R_{ab}-Cy5 was evaluated in DNase I, cell lysate, normal human serum, urine and saliva. LNA modified AuNR-R_{ab}-Cy5 shows much better stability than that without LNA (Figure S4). To avoid the effect of possible digestion on the experimental results, excessive free DNA H_1 and H_2 were transfected into the cells to ensure sufficient H_1 and H_2 available for CHA (Supporting Information). Therefore, AuNR-R_{ab}-Cy5, H_1 and H_2 could be safely delivered into living cells for subsequent survivin mRNA imaging. The ACHA nanoplatform was applied to intracellular survivin mRNA imaging for Hela, MCF-7, and MCF-10A cells. The three cells lines show various fluorescence signals. MCF-7 cells exhibit weaker fluorescence than Hela cells, but stronger than MCF-10A cells (Figure 4), suggesting the relative expression levels of survivin mRNA in the three cell lines. Quantitative reverse transcription-PCR analysis also reveals the survivin mRNA relative expression levels in the three cell lines (Figure S5 and S6).

To show whether the targeting delivery of transfection complex into cancer cells occurred, we have collected both normal cells (MCF-10A and 293T cells) and cancer cells (Hela and MCF-7 cells) incubated with transfection complex for the determination of Au in the cells by inductively coupled plasma optical emission spectrometry. 57-73% of the transfection complex were delivered into both the normal cells and the cancer cells (Figure S3), conforming the non-targeting delivery of the transfection complex. Due to the non-targeting delivery, the transfection complex for the specific fluorescence imaging of cancer cells merely results from the intracellular survivin mRNA triggering.

It was reported that survivin mRNA expression could be depressed by YM155.[33] So, we further applied the ACHA nanoplatform to intracellular survivin mRNA imaging in Hela cells with or without YM155. The Hela cells without YM155 shows stronger fluorescence than that with YM155 (Figure

S7). The results demonstrate the practicability of the ACHA nanoplatform for intracellular mRNA.

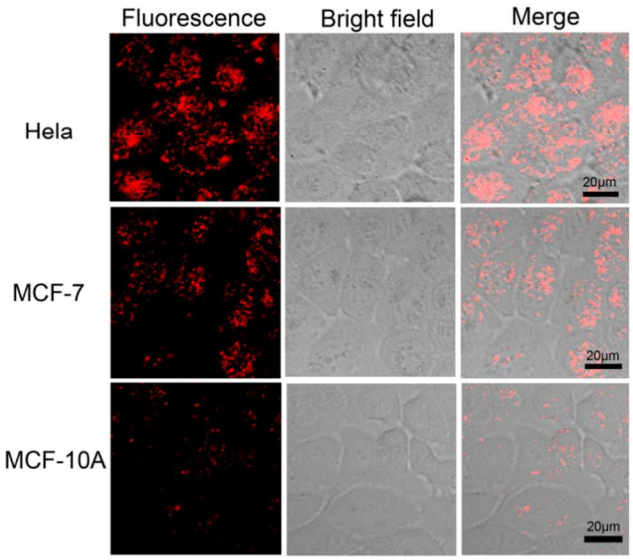

Figure 4. ACHA nanoplatform for living cell images. The fluorescence cell images were captured under the same conditions.

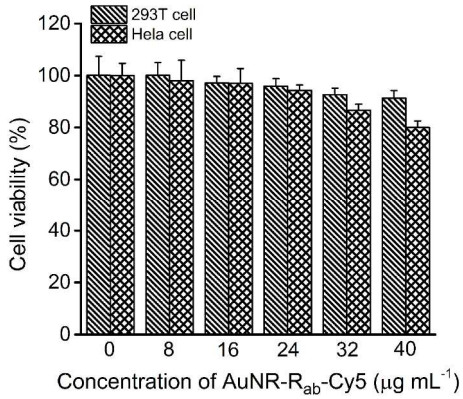

Figure 5. Cell viability of 293T and Hela cells after incubation with different concentrations of AuNR-R_{ab}-Cy5.

The cytotoxicity of the prepared AuNR-R_{ab}-Cy5 was evaluated on 293T cells (normal cells) and Hela cells (cancer cells). No obvious cytotoxicity was observed as the viability of 293T cells and Hela cells were over 80% even in the presence of 40 μg mL^{-1} AuNR-R_{ab}-Cy5 (Figure 5). The PTT efficacy of AuNR-R_{ab}-Cy5 was tested both in vitro and in vivo. The viability of Hela cells decreased as the AuNR-R_{ab}-Cy5 concentration increased under 808 nm laser irradiation (Figure 6A). Increase of the power density of the 808 nm laser irradiation also led to the decrease of the viability of the cancer cells (Figure 6B). The above results show a good in vitro PTT performance of AuNR-R_{ab}-Cy5.

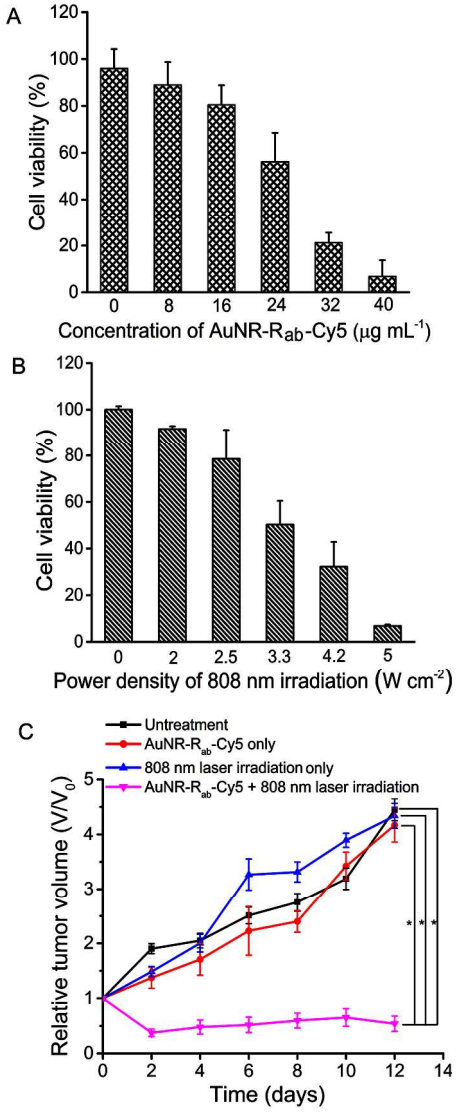

Figure 6. PTT performance of AuNR-R_{ab}-Cy5: (A) Effect of the concentrations of AuNR-R_{ab}-Cy5 under 808 nm laser irradiation (3.3 W cm^{-2}, 10 min) on the cell viability of Hela cells. (B) Effect of the power density of 808 nm laser irradiation on the cell viability of Hela cells in the presence of 24 μg mL^{-1} AuNR-R_{ab}-Cy5. (C) Relative tumor volume change of different groups of mice: untreatment, intratumorally injected with AuNR-R_{ab}-Cy5 (200 μg mL^{-1}, 100 μL) alone, 808 nm laser irradiation (3.3 W cm^{-2}, 10 min) alone, and intratumorally injected with AuNR-R_{ab}-Cy5 plus 808 nm laser irradiation. Tumor volumes were measured in a period of 12 days.

To further demonstrate the photothermal performance of AuNR-R_{ab}-Cy5 in vivo, tumor volumes on the mice of different groups were monitored for 12 days. The tumor volumes of the untreated mice, the mice treated with AuNR-R_{ab}-Cy5 alone and 808 nm laser irradiation alone obviously increased com-

pared with the original tumor volumes. In contrast, the tumor of the mice treated with AuNR-R_{ab}-Cy5 plus 808 nm laser irradiation were significantly suppressed in the period of 12 days (Figure 6C). These results indicate the excellent in vivo photothermal performance of AuNR-R_{ab}-Cy5.

In summary, we have proposed an ACHA theranostic nanoplatform for intracellular mRNA triggered fluorescence enhanced imaging guided PTT. The integrated CHA enables highly sensitive and specific imaging of intracellular mRNA, while the AuNRs provides high photothermal conversion efficiency for PTT. In addition, the low cytotoxicity of AuNR-R_{ab}-Cy5 endows good biocompatibility for theranostic application. The developed "off" to "on" ACHA theranostic nanoplatform not merely provides a sensitive and specific intracellular mRNA imaging method, but also an imaging guided high efficient PTT.

AUTHOR INFORMATION

Corresponding Author

*E-mail: xpyan@nankai.edu.cn. Fax: +86-22-23506075.

ORCID

Feng-Xia Su：0000-0001-9202-3792
Cheng-Xiong Yang：0000-0002-0817-2232
Xiu-Ping Yan：0000-0001-9953-7681

Notes

The authors declare no competing financial interest.

ACKNOWLEDGMENT

The authors appreciate the support from the National Natural Science Foundation of China (21435001) and Open Funds of the State Key Laboratory of Electroanalytical Chemistry (SKLEAC201705).

ASSOCIATED CONTENT

Supporting Information

The Supporting Information is available free of charge on the ACS Publications website.

Materials and chemicals, instrumentation, detailed experimental procedures and other supporting figures (PDF)

REFERENCES

(1) Schwarzenbach, H.; Hoon, D. S. B.; Pantel, K.; *Nat. Rev. Cancer* **2011**, *11*, 426-437.

(2) Del Pino, M.; Barrie, C. S.; Torné, A.; Marimon, L.; Gaber, J.; Sagasta, A.; Persing, D. H. *J. Ordi, Modern Pathology* **2015**, *28*, 312-320.

(3) Sueokaa, E.; Sueokaa, N.; Iwanagaa, K.; Satoa, A.; Sugab, K.; Hayashia, S.; Nagasawaa, K.; Nakachic, K.; *Lung Cancer* **2005**, *48*, 77-83.

(4) Tyagi, S. *Nat. Methods*, **2009**, *6*, 331-338.

(5) Bratu, D. P.; Cha, B. J.; Mhlanga, M. M.; Kramer, F. R.; Tyagi, S. *Proc. Natl. Acad. Sci. U. S. A.* **2003**, *100*, 13308-13313.

(6) Seferos, D. S.; Giljohann, D. A.; Hill, H. D.; Prigodich, A. E.; Mirkin, C. A. *J. Am. Chem. Soc.* **2007**, *129*, 15477-15479.

(7) Conde, J.; Rosa, J.; De la Fuente, J. M.; Baptista, P. V. *Biomaterials* **2013**, *34*, 2516-2523.

(8) Pan, W.; Yang, H.; Zhang, T.; Li, Y.; Li, N.; Tang, B. *Anal. Chem.* **2013**, *85*, 6930−6935.

(9) Ding, Q.; Zhan, Q.; Zhou, X.; Zhang, T.; Xing, D. *Small* **2016**, *12*, 5944-5953.

(10) Lin, L. S.; Cong, Z. X.; Cao, J. B.; Ke, K. M.; Peng, Q. L.; Gao, J.; Yang, H. H.; Liu, G.; Chen, X. *ACS Nano* **2014**, *8*, 3876-3883.

(11) Wu, D.; Song, G.; Li, Z.; Zhang, T.; Wei, W.; Chen, M.; He, X.; Ma, N. *Chem. Sci.* **2015**, *6*, 3839-3844.

(12) Gao, Y.; Qiao, G.; Zhuo, L.; Li, N.; Liu, Y.; Tang, B. *Chem. Commun.* **2011**, *47*, 5316-5318.

(13) Bustin, S. A. *J. Mol. Endocrinol* **2002**, *29*, 23-39.

(14) Nolan, T.; Hands, R. E; Bustin, S, A. *Nat. Protoc.* **2006**, *1*, 1559-1582.

(15) Zhao, W.; Ali, M. M.; Brook, M. A.; Li, Y. *Angew. Chem., Int. Ed.* **2008**, *47*, 6330-6337.

(16) Ali, M. M.; Li, F.; Zhang, Z.; Zhang, K.; Kang, D. K.; Ankrum, J. A.; Le, X. C.; Zhao, W.; *Chem. Soc. Rev.* **2014**, *43*, 3324-3341.

(17) Notomi, T.; Okayama, H.; Masubuchi, H.; Yonekawa, T.; Watanabe, K.; Amino, N.; Hase, T. *Nucleic Acids Res.* **2000**, *28*, e63.

(18) Wu, C.; Cansiz, S.; Zhang, L.; Teng, I-T.; Qiu, L.; Li, J.; Liu, Y.; Zhou, C.; Hu, R.; Zhang, T.; Cui, C.; Cui, L.; Tan, W. *J. Am. Chem. Soc.* **2015**, *137*, 4900-4903.

(19) Choi, H. M. T.; Chang, J. Y.; Trinh, L. A.; Padilla, J. E.; Fraser, S. E.; Pierce, N. A. *Nat. Biotechnol.* **2010**, *28*, 1208-1212.

(20) Choi, H. M. T.; Beck, V. A.; Pierce, N. A. *ACS Nano* **2014**, *8*, 4284-4294.

(21) Huang, J.; Wang, H.; Yang, X.; Yang, Y.; Quan, K.; Ying, L.; Xie, N.; Ou, M.; Wang, K. *Chem. Commun.* **2016**, *52*, 370-373.

(22) Wu, Z.; Liu, G.-Q.; Yang, X.-L.; Jiang, J.-H. *J. Am. Chem. Soc.* **2015**, *137*, 6829-6836.

(23) Tang, Y.; Zhang, X. L.; Tang, L. J.; Yu, R. Q.; Jiang, J. H. *Anal. Chem.* **2017**, *89*, 3445-3451.

(24) Yin, P.; Choi, H. M. T.; Calvert, C. R.; Pierce, N. A. *Nature* **2008**, *451*, 318-322.

(25) Zang, Y.; Lei, J.; Ling, P.; Ju, H. *Anal. Chem.* **2015**, *87*, 5430−5436

(26) Li, B.; Ellington, A. D.; Chen, X. *Nucleic Acids Res.* **2011**, *39*, e110.

(27) Jang, B.; Kim, Y. S.; Choi, Y. *Small* **2011**, *7*, 265-270.

(28) Zhang, Z.; Wang, J.; Chen, C. *Theranostics* **2013**, *3*, 223-238.

(29) Joo, J. H.; Lee, J.-S. *Anal. Chem.* **2013**, *85*, 6580−6586

(30) Nikoobakht, B.; El-Sayed, M. A. *Chem. Mater.* **2003**, *15*, 1957-1962.

(31) Li, J.; Zhu, B.; Zhu, Z.; Zhang, Y.; Yao, X.; Tu, S.; Liu, R.; Jia, S.; Yang, C. J. *Langmuir* **2015**, *31*, 7869-7876.

(32) Altieri, D. C. *Oncogene* **2003**, *22*, 8581-8589.

(33) Nakahara, T.; Takeuchi, M.; Kinoyama, I.; Minematsu, T.; Shirasuna, K.; Matsuhisa, A.; Kita, A.; Tominaga, F.; Yamanaka, K.; Kudoh, M.; Sasamata, M. *Cancer Res.* **2007**, *67*, 8014.

For TOC only